Available online at www.sciencedirect.com
SCIENCE DIRECT®
Optical Materials xxx (2005) xxx–xxx
OPTICAL Materials
www.elsevier.com/locate/optmat

Luminescence of erbium-doped bismuth–borate glasses

Isabella-Ioana Oprea, Hartmut Hesse, Klaus Betzler *

Fachbereich Physik, Universität Osnabrück, D-49069 Osnabrück, Germany

Received 26 May 2005; accepted 12 July 2005

Abstract

Absorption and luminescence properties of erbium ions in the binary glass system bismuth oxide (Bi_2O_3)–boric oxide (B_2O_3) are measured for the composition range 25–65 mol% Bi_2O_3. A Judd–Ofelt analysis of the typical erbium bands in the absorption spectra reveals comparably high Judd–Ofelt coefficients. This indicates a substantial mixing of other electronic configuration into the $4f^N$ configuration by the random crystal fields in the glasses. All coefficients are decreasing with increasing Bi_2O_3 content, this effect being most pronounced with Ω_2. Luminescence decay times and radiative efficiencies show an expressed dependence on the glass composition. Radiative efficiencies of all luminescence bands increase with increasing Bi_2O_3 content—accompanied, however, by a slight narrowing of the bands. Except the common luminescence bands of erbium, upconversion luminescence at a wavelength of 0.54 μm could be detected.

PACS: 42.70.Ce; 78.55.Qr

Keywords: Erbium doping; Bismuth–borate glass; Luminescence

1. Introduction

Since about 40 years, rare earth ions like Er^{3+} have attracted much interest as luminescence centers in crystals as well as in glasses [1–6]. Presently, special attention is paid to erbium due to its emission band at 1.53 μm which makes it an ideal element for applications in the field of optical data transmission (erbium-doped fiber amplifier). Luminescence properties of Er^{3+} have been studied in crystalline hosts including garnets and related materials [7–11] where the suitability for lasers in the near infrared range has been demonstrated. Glassy host materials investigated include silicate glasses [12,13], germanate glasses [14], phosphate glasses [15,16], sulphide glasses [17,18], tellurite glasses [19] as well as more complicated glass systems like $Na_2O \cdot Ca_3Al_2Ge_3O_{12}$ [20] or ZBLAN ($ZrF_4 \cdot BaF_2 \cdot LaF_3 \cdot AlF_3 \cdot NaF$) [21], probably better suited for fiber amplifiers.

In glasses, various relevant properties—as e.g., the refractive index—can be tuned by the addition of heavy ions like lead or bismuth. Thus systems consisting of a light and a heavy component, preferably allowing for a broad composition range, are most suitable for applications where a wide tunability of the properties is desired. One of these systems is the binary phase boric oxide (B_2O_3)–bismuth oxide (Bi_2O_3) [22]. Glasses can be prepared in this system with Bi_2O_3 contents ranging from about 25–65 mol%. Several authors have recently studied the properties of bismuth borate glasses, undoped [23], Er^{3+}-doped [24] or Nd^{3+}-doped [25], however, in a restricted composition range. Becker could show, that the refractive index can be widely

* Corresponding author. Tel.: +49 541 969 2636; fax: +49 541 969 12636.
E-mail address: klaus.betzler@uos.de (K. Betzler).

0925-3467/$ - see front matter © 2005 Published by Elsevier B.V.
doi:10.1016/j.optmat.2005.07.004

varied [23], Chen et al. proved that high luminescence efficiencies are possible—especially in Nd^{3+}-doped glass [25]. Tanabe et al. [26] showed for Er^{3+} doped $Bi_2O_3 \cdot B_2O_3 \cdot SiO_2$ glasses that the luminescence lifetime and efficiency decrease with increasing B_2O_3 content. Similar results were found by Yang et al. [27] for $Bi_2O_3 \cdot B_2O_3 \cdot Na_2O$ glasses.

In this work, we present a comprehensive analysis of the optical properties—especially the luminescence properties—of Er^{3+} doped bismuth borate glasses for the complete composition range spanning from 25 to 65 mol% bismuth oxide. Besides the refractive indices and the absorption properties, the influence of the composition on the luminescence linewidth and the luminescence efficiency is studied.

2. Experimental

Samples of Er^{3+} doped bismuth borate glasses $(Er_2O_3)_y((Bi_2O_3)_x(B_2O_3)_{1-x})_{1-y}$ with compositions spanning the range $x = 0.25 \ldots 0.65$ and $y = 0.0025$ were fabricated from melts of corresponding compositions. The melts were thoroughly homogenized at a temperature of ≈1000 K and then cooled down to room temperature at a rate of 100 K per hour. To study the influence of higher Er^{3+} doping, in addition, samples with $y = 0.0075$ and $y = 0.025$ were prepared for $x = 0.25$.

For the absorption measurements, a Bruins Omega 10 spectrometer was used working in the near ultraviolet, visible, and near infrared spectral region. The absorption data were measured on plate-shaped samples with a thickness of approximately 1 mm. The data were corrected for reflection using previously measured refractive index values of the same samples [28]. For the correction, the Sellmeier fit formula provided there for a wavelength range from 0.4 to 1.53 μm was applied. From this fit formula, also all refractive index data necessary for calculations were derived.

Luminescence measurements were performed in reflection geometry on platelet samples using several setups. For the spectra at 1.53 μm, a 1.48 μm or a 0.8 μm laser diode was used for excitation, an Amko monochromator and a suitable photodiode for detection. For all other spectra, a 0.8 μm semiconductor laser working in CW mode was applied as excitation source. The detection system consisted of a Jobin-Yvon TRIAX 180 spectrometer combined with either an infrared, red or green sensitive photomultiplier, depending on the spectral region of the respective measurement. For the decay measurements the samples were excited by a 0.8 μm or a 1.48 μm semiconductor laser in pulsed mode, appropriate photodiodes and photomultipliers rendered the time dependence of the luminescence.

3. Results and discussion

3.1. Absorption spectra and Judd–Ofelt analysis

For the short wavelength absorption edge of undoped bismuth borate glasses a strongly expressed dependence on the Bi_2O_3 content had been found previously [28]. Doped glasses show a similar behavior for the absorption edge. The typical erbium absorption bands, however, exhibit only a very slight yet expressed dependence on the glass composition. This is shown in Fig. 1 for the two compositions $x = 0.25$ and $x = 0.65$ (erbium content $y = 0.0025$).

Electric dipole transitions between two states of $4f^N$ configuration of rare earth ions, which are forbidden for free ions, become allowed in the crystal field by mixing into the $4f^N$ configuration another configuration ($4f^{N-1}5d^1$) of opposite parity. The matrix elements of the electric dipole operator are calculated by considering the crystal field as a first-order perturbation.

According to the Judd–Ofelt theory [29,30], the effect of the crystal field can be described by three intensity parameters $\Omega_{2,4,6}$. The line strength for the electric dipole transition S^{ed} then is given by

$$S^{ed}[(S,L)J;(S',L')J'] = \sum_{t=2,4,6} \Omega_t |\langle (S,L)J||U^{(t)}||(S',L')J'\rangle|^2, \quad (1)$$

where Ω_t are the Judd–Ofelt parameters, $U^{(t)}$ are the unit tensor operators, and $(S,L)J$ and $(S',L')J'$ represent the initial and final states of the transition.

For magnetic dipole transitions, the line strength S^{md} is defined as

$$S^{md}[(S,L)J;(S',L')J'] = \frac{1}{4m^2c^2} |\langle (S,L)J||L+2S||(S',L')J'\rangle|^2 \quad (2)$$

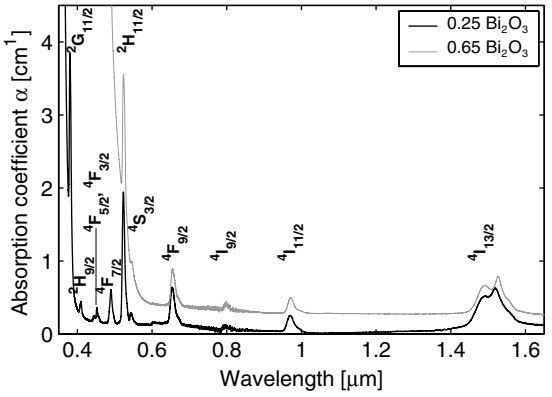

Fig. 1. Absorption spectra of Er^{3+} doped bismuth borate glasses for two glass compositions ($x = 0.25$ and $x = 0.65$, for better visibility the spectrum for $x = 0.65$ is shifted upwards). The absorption bands correspond to transitions from the erbium ground state $^4I_{15/2}$ to the excited states assigned.

with m—electron mass and c—velocity of light. Numerical values for the matrix elements in Eqs. (1) and (2) can be calculated according to Carnall et al. [31] and Weber [7]. The integral intensity over an absorption band then can be written as

$$\int_{\text{band}} \alpha \, d\lambda = \frac{2\pi^2 e^2 \bar{\lambda} \rho}{3\varepsilon_0 ch(2J+1)n^2} \cdot \left(\frac{n(n^2+2)^2}{9} S^{\text{ed}} + n^3 S^{\text{md}} \right), \quad (3)$$

where α is the absorption coefficient, $\bar{\lambda}$ the mean absorption wavelength, e the electron charge, ρ the erbium concentration, ε_0 the vacuum permittivity, h Planck's constant, $(2J+1)$ the multiplicity of the ground level, and n the refractive index.

Using Eq. (3) the Judd–Ofelt coefficients were calculated applying a least-squares fit procedure to the integral absorption intensities of the various bands in the measured absorption spectra. The results are listed in Table 1.

All Judd–Ofelt coefficients exhibit comparably high values. While Ω_4 is approximately constant, Ω_2 and Ω_6 are decreasing with increasing Bi_2O_3 content. This indicates that short range structural disorder effects—expressed by Ω_2—are decreasing, whereas covalency effects in the Er–O bonds—showing up in Ω_6—are increasing with increasing Bi_2O_3 content. The values for the Judd–Ofelt coefficients previously given by Chen et al. [24] for compositions between 0.25 and 0.45 differ slightly from our values but show the same trends. The deviations may be attributed to differences in the reflection corrections applied to the absorption measurements. For these corrections, we used the wavelength dependent Sellmeier description of the refractive indices [28] whereas Chen et al. did not apply such a correction to their measurements.

3.2. Luminescence at 1.53 μm

For applications in optical communication systems most important is the emission band at 1.53 μm arising from the transition $^4I_{13/2} \rightarrow {}^4I_{15/2}$. This emission can be pumped through the corresponding absorption transition $^4I_{15/2} \rightarrow {}^4I_{13/2}$ using an appropriate semiconductor laser, e.g., at 1.48 μm.

Table 1
Calculated Judd–Ofelt parameters Ω_t (in units of 10^{-24} m^2) as a function of the glass composition (Bi_2O_3 content) for an Er_2O_3 content of $y = 0.0025$

Bi_2O_3 content	Ω_2	Ω_4	Ω_6
0.25	4.58	1.44	1.53
0.35	3.72	1.16	1.15
0.45	3.56	1.11	1.29
0.55	3.45	1.18	1.05
0.65	2.56	1.23	0.82

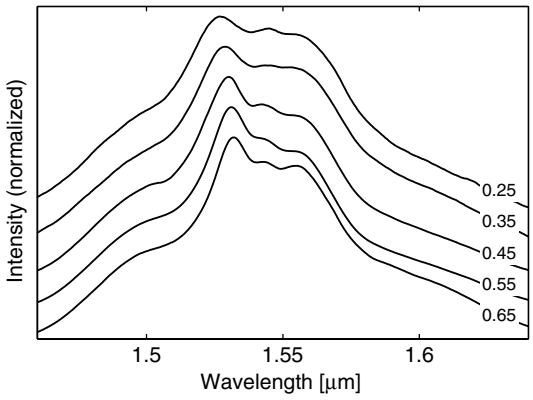

Fig. 2. 1.53 μm emission spectra of Er^{3+} ions in bismuth borate glass samples of different compositions (Bi_2O_3 content indicated at the right side of the spectra). Pump wavelength was 0.8 μm.

For the evaluation of the spectroscopic parameters of the 1.53 μm emission band and their composition dependence the samples were pumped, however, by a 0.8 μm laser to avoid any influence of the pumping light on the measured spectra. The composition dependence of the emission spectra is shown in Fig. 2. Low Bi_2O_3 content favors comparably broad and flat spectra, increasing Bi_2O_3 content leads to narrower, more structured bands and, furthermore, to a slight red shift of the bands. The slight but distinct change of the luminescence band shape between 0.35 and 0.45 compositions might be attributed to a change in the glass microstructure. Indications for such a change to occur at a composition of approximately 0.40 are found in differential thermal analysis heating experiments carried out by Becker [23] on bismuth borate glasses in this composition range.

The overall shapes of our luminescence bands differ from those measured recently by Chen et al. [24]. This might be due to a different spectral response of the detectors used in the measurements. As for our measurements an InGaAs photodiode with flat response in the spectral region near 1.5 μm was used, the shapes seem to be reliable. This is further confirmed by the calculation of the band shapes from the absorption bands using McCumber's theory [33] as shown in the subsequent section.

As characterizing spectroscopic parameters the typical (effective) width of the bands, defined as

$$\Delta\lambda = \int I(\lambda) d\lambda / I_{\max} \quad (4)$$

the position of the maximum λ_{peak}, and the center of mass wavelengths $\bar{\lambda}$ of the emission bands, given by

$$\bar{\lambda} = \int \lambda I(\lambda) d\lambda \Big/ \int I(\lambda) d\lambda \quad (5)$$

Table 2
Line width $\Delta\lambda$, peak wavelength λ_{peak}, and center of mass wavelength $\bar{\lambda}$ for the 1.53 μm emission band in erbium doped bismuth borate glass as a function of the composition (Bi_2O_3 content)

Bi_2O_3 content	$\Delta\lambda$ (μm)	λ_{peak} (μm)	$\bar{\lambda}$ (μm)
0.25	0.0856	1.5271	1.5418
0.35	0.0824	1.5289	1.5440
0.45	0.0748	1.5301	1.5425
0.55	0.0712	1.5311	1.5429
0.65	0.0758	1.5319	1.5463

were calculated from the measured emission spectra. The data are listed in Table 2.

The red shift, found for increasing Bi_2O_3 content both in the peak wavelength and in the center of mass wavelength of the band, can be attributed to the nephelauxetic effect typical for rare earth ions in different environments. It indicates an increase in the covalency of the Er–O bonds with increasing Bi_2O_3 content. Width and flatness of the band—especially at low Bi_2O_3 content—underline the suitability of these glasses for amplifier applications. The trend in the emission band width is caused by an increasing optical basicity of the host glass with increasing Bi_2O_3 content [32].

The shape of the bands, furthermore, reflects the trends in the Judd–Ofelt parameters. While the narrow peak at the low wavelength side of the emission band is due to the magnetic dipole transition—allowed and thus independent of the ligand field, the broader structure in the band is governed by electric dipole transitions—forbidden and thus dependent from the ligand field. According to Weber [7] the line strength S^{ed} for this band is obtained from the Judd–Ofelt parameters by

$$S^{ed}[^4I_{13/2};{}^4I_{15/2}] = 0.019\Omega_2 + 0.118\Omega_4 + 1.462\Omega_6. \quad (6)$$

Ω_6 is the dominating factor there-in, thus the trend in Ω_6 (see Table 1) correlates to the trend in the spectrum shape.

3.3. Radiative efficiencies

Besides line width and shape, for amplifier applications the stimulated emission cross-section of a transition and its radiative quantum efficiency are of fundamental importance. Stimulated emission cross-sections and the spectral shape of the emission bands can be calculated from the corresponding absorption bands by applying McCumber's theory [33]. A typical result is shown in Fig. 3, measured absorption and calculated stimulated emission cross-sections are plotted for the $^4I_{13/2} \leftrightarrow {}^4I_{15/2}$ transition in a glass with 0.25 Bi_2O_3 content. To get an estimate for the accuracy of the spectral shape calculation, the measured emission band is plotted, too. From the comparison, an accuracy of about 5% for the McCumber calculation can be estimated.

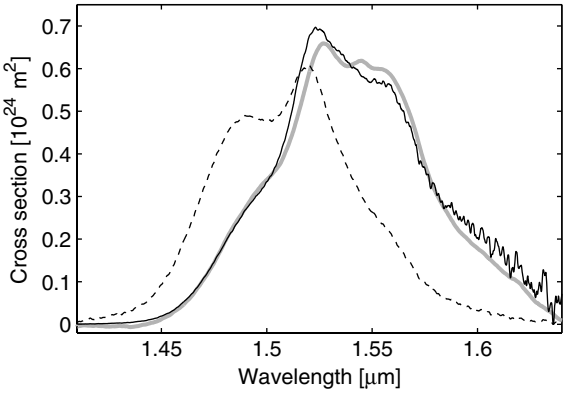

Fig. 3. $^4I_{15/2} \rightarrow {}^4I_{13/2}$ absorption band of Er^{3+} in a glass with 0.25 Bi_2O_3 content (dashed). Applying McCumber's theory, the corresponding stimulated emission cross-section is calculated (solid black). The gray curve represents the measured emission spectrum of the $^4I_{13/2} \rightarrow {}^4I_{15/2}$ transition.

In another way to derive the stimulated emission cross-sections the spontaneous emission probabilities can be used which are calculated as sum of electric and magnetic dipole contributions from the respective line strengths S^{ed} and S^{md} [34]

$$A_{J'J} = A^{ed}_{J'J} + A^{md}_{J'J} = \frac{16\pi^3 e^2}{3\varepsilon_0 h(2J'+1)\lambda^3}\left\{\frac{n(n^2+2)^2}{9}S^{ed}_{J'J} + n^3 S^{md}_{J'J}\right\} \quad (7)$$

for the transition between excited state J' with multiplicity $(2J'+1)$ and ground state J. The line strengths S can be calculated according to Eqs. (1) and (2) using the Judd–Ofelt parameters determined for the system.

The stimulated emission cross-section σ_e for the transition $J' \rightarrow J$ then is given by [35]

$$\sigma_e[J';J] = \frac{\bar{\lambda}^4 A_{J'J}}{8\pi c n^2 \Delta\lambda}. \quad (8)$$

Using both methods described, we calculated the stimulated emission cross-sections for the $^4I_{13/2} \rightarrow {}^4I_{15/2}$ transition. The values are summarized in Table 3, column I gives the maximum values of the McCumber bands, column II the results of the derivation from the line

Table 3
Stimulated emission cross-section for the $^4I_{13/2} \rightarrow {}^4I_{15/2}$ transition of Er^{3+} in bismuth borate glasses of different compositions

Bi_2O_3 content	Stimulated emission cross-section (10^{-24} m^2)			
	I	II	III	IV
0.25	0.70	0.66	0.72	0.67
0.35	0.77	0.62	0.84	0.70
0.45	0.83	0.79	0.94	0.71
0.55	0.86	0.78	–	–
0.65	0.82	0.67	–	–

I: McCumber calculation, II: derived from the line strengths, III: Ref. [24]—0.1% Er_2O_3, IV: Ref. [24]—0.5% Er_2O_3.

strengths. For comparison, data published by Chen et al. [24] for two different erbium concentrations are given in columns III and IV.

From the spontaneous emission probability A (Eq. (7)) the radiative lifetime $\tau_r = A^{-1}$ for a transition can be derived. A comparison with the total lifetime τ_t yields the radiative quantum efficiency

$$\eta = \tau_t/\tau_r. \quad (9)$$

The total lifetime can be determined experimentally by measuring the luminescence decay for the respective transitions. Typical measured decay curves are shown in Fig. 4. The linear functional relationship in the semi-logarithmic plot proves a strictly exponential behavior which can be described by a single time constant τ_t unique for each of the decay curves.

Decay curves have been measured for the $^4I_{11/2} \rightarrow {}^4I_{15/2}$ transition at 0.97 μm with 0.8 μm excitation and for the $^4I_{13/2} \rightarrow {}^4I_{15/2}$ transition at 1.53 μm with 1.48 μm excitation for all compositions. The results—calculated radiative lifetimes τ_r, experimentally determined total lifetimes τ_t, and radiative quantum efficiencies η—are summarized in Table 4.

The results show that the radiative lifetimes are slightly decreasing with increasing Bi_2O_3 content whereas the total lifetimes increase. This leads to an increase in the radiative quantum efficiencies with increasing Bi_2O_3 content up to nearly 40% for the 1.53 μm luminescence in the glass with the highest Bi_2O_3 content. Chen et al. [24] measured the decay times for compositions between 0.25 and 0.45 for the 1.53 μm band. They found slightly lower values which might be due to the different excitation mechanisms (they used an excitation wavelength of 0.97 μm whereas we used 1.48 μm).

The trend in the radiative efficiencies can be explained by the nonradiative transition probabilities. One of the most dominant of these transition processes for rare-earth ions in glasses with high phonon energy is multi-phonon relaxation. According to Layne et al. [36] the probabilities for multi-phonon processes depend exponentially on the phonon energies. B_2O_3 host structures contribute high phonon energies, Bi_2O_3 structures considerably lower ones. Thus in B_2O_3 rich glasses high nonradiative transition probabilities, i.e., low radiative efficiencies, are found, whereas in the Bi_2O_3 rich glasses the nonradiative transition probabilities decrease, enabling higher radiative efficiencies.

Table 4
Radiative lifetimes, total lifetimes, and radiative efficiencies for the $^4I_{11/2} \rightarrow {}^4I_{15/2}$ and the $^4I_{13/2} \rightarrow {}^4I_{15/2}$ transitions (0.97 μm and 1.53 μm) of Er^{3+} in glasses of different compositions (Bi_2O_3 content)

Bi_2O_3 content	$^4I_{11/2} \rightarrow {}^4I_{15/2}$ (0.97 μm)			$^4I_{13/2} \rightarrow {}^4I_{15/2}$ (1.53 μm)		
	τ_r (ms)	τ_t (ms)	η (%)	τ_r (ms)	τ_t (ms)	η (%)
0.25	3.36	0.61	18.2	3.98	0.52	13.1
0.35	3.44	0.65	18.5	3.92	0.68	17.5
0.45	2.60	0.66	25.3	3.03	0.89	29.5
0.55	2.62	0.69	26.3	2.97	1.03	34.6
0.65	2.88	0.71	24.8	3.05	1.13	37.2

3.4. Upconversion luminescence

Previous investigations were unable to detect upconversion luminescence in Er^{3+} doped bismuth borate glasses, several reasons were discussed [24]. Using 0.8 μm laser excitation combined with sensitive photon-counting detection techniques and prolongated integration times, we at last succeeded in demonstrating such a luminescence band at 0.54 μm, yet at fairly low intensity. The shape of the luminescence band is plotted in Fig. 5 together with its pump-intensity dependence. The slope of 1.8 found indicates a two-step excitation process for the upconversion luminescence.

In order to find the explanation for the unusually low intensities we calculated the radiative lifetimes for the transition $^4S_{3/2} \rightarrow {}^4I_{15/2}$ responsible for the measured upconversion luminescence at 0.54 μm. The values vary

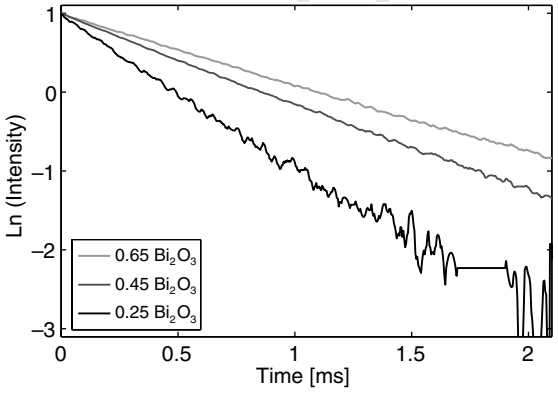

Fig. 4. Luminescence decay for the $^4I_{13/2} \rightarrow {}^4I_{15/2}$ transition of Er^{3+} in bismuth borate glasses of different compositions.

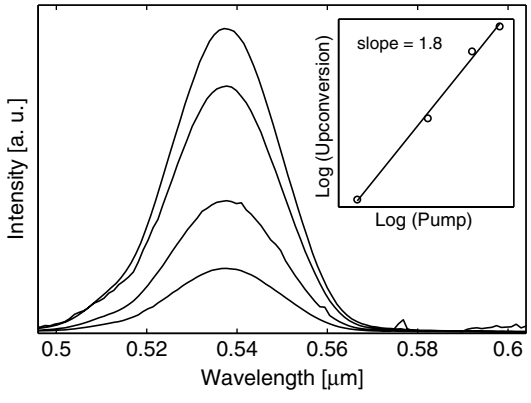

Fig. 5. Upconversion luminescence in Er^{3+} doped bismuth borate glass (Bi_2O_3 content 0.25). In the inset the dependence of the upconversion intensity on pump intensity is sketched.

from 0.3 ms to 0.25 ms for the Bi_2O_3 content varying from 0.25 to 0.65. In contrast to this, the measured decay times for this luminescence band (when excited with pulsed 0.53 μm laser light) lie at approximately 100 ns [36]. Thus the radiative quantum efficiencies for this transition are in the order of only 0.03%. This extremely low value is due to a high nonradiative transition rate from the $^4S_{3/2}$ level to the $^4F_{9/2}$ level of Er^{3+} caused by the high phonon energies of the B_2O_3 host structures [36].

3.5. Higher doping

To study the effect of higher doping, absorption and emission spectra for samples with tripled and 10-fold erbium content have been measured. For the concentration range investigated, all absorption bands scaled linearly with the erbium concentration. That means unchanged Judd–Ofelt parameters.

The measured luminescence decay times, however, showed a slight decrease—from 0.61 ms to 0.58 ms for the 0.97 μm band and from 0.52 ms to 0.45 ms for the 1.53 μm band—for the erbium content increasing by a factor of ten. This corresponds to a decrease in the radiative quantum efficiencies from 18.2% to 17.1% and from 13.1% to 11.4%, respectively.

4. Conclusions

Optical properties—including refractive indices, absorption and emission spectra, decay times of selected transitions, and upconversion luminescence—of erbium doped bismuth borate glasses have been measured for a wide composition range. Varying the Bi_2O_3 content from 0.25 to 0.65, the refractive index of the glasses can be tuned between 1.8 and 2.3. For the description of the refractive indices in the wavelength range from 0.4 to 1.5 μm and in the full composition range a generalized Sellmeier formula is provided. From the absorption spectra, the Judd–Ofelt parameters are derived for all glass compositions. They can be used to calculate oscillator strengths, line strengths, transition probabilities, radiative lifetimes, and stimulated emission cross-sections—applying the usual formulas.

From the comparison between the calculated radiative lifetimes and the measured luminescence decay times the radiative quantum efficiencies for the $^4I_{11/2} \rightarrow {}^4I_{15/2}$ and the $^4I_{13/2} \rightarrow {}^4I_{15/2}$ transitions (0.97 μm and 1.53 μm, respectively) were derived. The maximum quantum efficiency of nearly 40% was found for the 1.53 μm transition in the glass with a Bi_2O_3 content of 0.65. The maximum linewidth of this transition, 0.093 μm, however, was obtained for a bismuth content of 0.25. Stimulated emission cross-sections for the $^4I_{13/2} \rightarrow {}^4I_{15/2}$ transition vary from about $0.75 \times 10^{-24}\,m^2$ for low to about $0.60 \times 10^{-24}\,m^2$ for high Bi_2O_3 content.

Upconversion luminescence at 0.54 μm could be demonstrated, however with extremely low intensity. The reasons for this are nonradiative multi-phonon transition processes, depleting the $^4S_{3/2}$ level, which are highly efficient in borate glasses due to the high phonon energies of the borate host structures.

Erbium doped bismuth borate glasses have thus been proven to be interesting materials for large range of optical applications like fiber amplifiers or lasers. Varying the composition of the host glass, the application-relevant parameters can be widely adjusted to suit the needs of the particular application.

Acknowledgments

The work was supported by the Federal State of Niedersachsen within the Graduate School 'Synthesis and Characterization of Surfaces and Interfaces Assembled from Clusters and Molecules'.

References

[1] E. Snitzer, R. Woodcock, J. Opt. Soc. Am. 55 (1965) 608.
[2] E. Snitzer, R. Woodcock, Appl. Phys. Lett. 6 (1965) 45.
[3] E. Snitzer, R.F. Woodcock, J. Segre, IEEE J. Quantum Electron. QE 4 (1968) 360.
[4] M.J. Weber, M. Bass, T.E. Varitimos, D.P. Bua, IEEE J. Quantum Electron. QE 9 (1973) 1079.
[5] S. Tanabe, Glass Sci. Technol.—Glastech. Ber. 74 (2001) 67.
[6] S. Tanabe, C.R. Chim. 5 (2002) 815.
[7] M.J. Weber, Phys. Rev. 157 (1967) 262.
[8] M.J. Weber, Phys. Rev. 156 (1967) 231.
[9] M.J. Weber, M. Bass, G.A. Demars, J. Appl. Phys. 42 (1971) 301.
[10] D.K. Sardar, W.M. Bradley, J.J. Perez, J.B. Gruber, B. Zandi, J.A. Hutchinson, C.W. Trussell, M.R. Kokta, J. Appl. Phys. 93 (2003) 2602.
[11] D.K. Sardar, C.C. Russell, R.M. Yow, J.B. Gruber, B. Zandi, E.P. Kokanyan, J. Appl. Phys. 95 (2004) 1180.
[12] R. Woodcock, E. Snitzer, J. Opt. Soc. Am. 55 (1965) 608.
[13] J. Yang, S. Dai, N. Dai, S. Xu, L. Wen, L. Hu, Z. Jiang, J. Opt. Soc. Am. B 20 (2003) 810.
[14] Z.M. Yang, S.Q. Xu, L.L. Hu, Z.H. Jiang, J. Opt. Soc. Am. B—Opt. Phys. 21 (2004) 951.
[15] R. Francini, F. Giovenale, U.M. Grassano, Radiat. Eff. Defects Solids 149 (1999) 137.
[16] R. Francini, F. Giovenale, U.M. Grassano, P. Laporta, S. Taccheo, Opt. Mater. 13 (2000) 417.
[17] Y. Guimond, J.L. Adam, A.M. Jurdyc, H.L. Ma, J. Mugnier, B. Jacquier, J. Non-Cryst. Solids 257 (1999) 378.
[18] T.Y. Ivanova, A.A. Man'shina, A.V. Kurochkin, Y.S. Tver'yanovich, V.B. Smirnov, J. Non-Cryst. Solids 298 (2002) 7.
[19] H. Lin, K. Liu, E.Y.B. Pun, T.C. Ma, X. Peng, Q.D. An, J.Y. Yu, S.B. Jiang, Chem. Phys. Lett. 398 (2004) 146.
[20] H. Lin, E.Y.B. Pun, S.Q. Man, X.R. Liu, J. Opt. Soc. Am. B—Opt. Phys. 18 (2001) 602.
[21] Y.D. Huang, M. Mortier, F. Auzel, Opt. Mater. 17 (2001) 501.
[22] E.M. Levin, C.L. Mcdaniel, J. Am. Ceram. Soc. 45 (1962) 355.
[23] P. Becker, Cryst. Res. Technol. 1 (2003) 74.

[24] Y. Chen, Y. Huang, M. Huang, R. Chen, Z. Luo, Opt. Mater. 25 (2004) 271.
[25] Y. Chen, Y. Huang, M. Huang, R. Chen, Z. Luo, J. Am. Ceram. Soc. 88 (2005) 19.
[26] S. Tanabe, N. Sugimoto, S. Ito, T. Hanada, J . Lumin. 87 (9) (2000) 670.
[27] J.H. Yang, S.X. Dai, Y.F. Zhou, L. Wen, L.L. Hu, Z.H. Jiang, J. Appl. Phys. 93 (2003) 977.
[28] I.-I. Oprea, H. Hesse, K. Betzler, Opt. Mater. 26 (2004) 235.
[29] B.R. Judd, Phys. Rev. 127 (1962) 750.
[30] G.S. Ofelt, J. Chem. Phys. 37 (1962) 511.
[31] W.T. Carnall, P.R. Fields, B.G. Wybourne, J. Chem. Phys. 42 (1965) 3797.
[32] N. Sugimoto, S. Tanabe, J. Ceram. Soc. Jpn. 113 (2005) 120.
[33] D.E. McCumber, Phys. Rev. 136 (1964) A954.
[34] R.D. Peacock, in: J.D. Dunitz, P. Hemmerich, R.H. Holm, J.A. Ibers, C.K. Jorgensen, J.B. Neilands, D. Reinen, R.J.P. Williams (Eds.), Structure and Bonding, 22, Springer, Berlin, 1975, p. 83.
[35] A.P. Thorne, U. Litzén, S. Johansson, Spectrophysics, Principles and Applications, Springer, Berlin, Heidelberg, 1999.
[36] C.B. Layne, W.H. Lowdermilk, M.J. Weber, Phys. Rev. B 16 (1977) 10.